Article

Proof-of-Concept Quantitative Monitoring of Respiration Using Low-Energy Wearable Piezoelectric Thread

Kenta Horie [1], Muhammad Salman Al Farisi [1,*], Yoshihiro Hasegawa [1], Miyoko Matsushima [2], Tsutomu Kawabe [2] and Mitsuhiro Shikida [1]

[1] Department of Biomedical Information Sciences, Hiroshima City University, Hiroshima 731-3194, Japan
[2] Division of Host Defense Sciences, Omics Health Sciences, Department of Integrated Health Sciences, Graduate School of Medicine, Nagoya University, Nagoya 461-8673, Japan
* Correspondence: alfarisi@hiroshima-cu.ac.jp

Abstract: Currently, wearable sensors can measure vital sign frequencies, such as respiration rate, but they fall short of providing quantitative data, such as respiratory tidal volume. Meanwhile, the airflow at the mouth carries both the frequency and quantitative respiratory signals. In this study, we propose a method to calibrate a wearable piezoelectric thread sensor placed on the chest using mouth airflow for accurate quantitative respiration monitoring. Prior to human trials, we introduced an artificial ventilator as a test subject. To validate the proposed concept, we embedded a miniaturized tube airflow sensor at the ventilator's outlet, which simulates human respiration, and attached a wearable piezoelectric thread to the piston, which moves periodically to mimic human chest movement. The integrated output readings from the wearable sensor aligned with the airflow rate measurements, demonstrating its ability to accurately monitor not only respiration rate but also quantitative metrics such as respiratory volume. Finally, tidal volume measurement was demonstrated using the wearable piezoelectric thread.

Keywords: micro-electro mechanical systems (MEMS); airflow sensor; piezoelectric sensor; wearable; textile

1. Introduction

The advent of wearable sensors has ushered in a new era in health monitoring, providing unprecedented opportunities for continuous and real-time tracking of various physiological parameters [1,2]. These devices, seamlessly integrated into everyday items such as smartwatches, fitness trackers, patches, and smart clothing, offer a non-intrusive and user-friendly means to monitor and manage health [3–6]. Wearable sensors in health monitoring enable early detection of potential health issues, support chronic disease management, and facilitate personalized healthcare, ultimately improving patient outcomes and reducing healthcare costs. By collecting and analyzing data continuously, wearable sensors provide valuable insights that traditional, periodic monitoring methods cannot offer, allowing for more timely and informed medical interventions.

Among the many applications of wearable sensors, respiration monitoring stands out as particularly vital [4,7]. Accurate and continuous monitoring of respiratory parameters is crucial for managing and detecting conditions such as asthma, chronic obstructive pulmonary disease (COPD), and sleep apnea [8–10]. Wearable devices equipped with respiration sensors track breathing patterns, respiratory rate, and even the composition of exhaled breath, providing comprehensive data on an individual's respiratory health [11–13]. These devices leverage advanced technologies, including accelerometers, gyroscopes, and stretchable sensors, to measure the mechanical aspects of breathing, such as chest and abdomen movements [14–16]. Additionally, some wearable sensors analyze exhaled breath for volatile organic compounds, providing insights into metabolic changes and potential respiratory conditions [17].

Despite the advancements in respiration monitoring using wearable devices, several challenges still need to be overcome. One significant challenge is that the monitoring capabilities of most of these devices are often constrained to frequency-based measurements [10,18]. Current commercially available wearable sensors are unable to evaluate quantitative magnitudes such as respiratory tidal volume accurately. This limitation arises because such quantitative measurements depend on various attachment conditions, such as the sensor's location on the human body surface and the attachment strength, which can vary significantly between individuals. To obtain accurate quantitative values from these sensors, the output signal must be calibrated against the actual respiration waveforms of each user periodically. However, such calibrations typically require expensive medical equipment, such as spirometers [19,20]. The complexity and need for direct supervision by medical personnel make it impractical to incorporate these calibrations into daily life. Addressing these challenges is crucial for enhancing the performance and utility of wearable health devices.

For quantitative measurement of respiration, mask sensors and portable spirometry have been proposed [12,13,20]. However, wearing these sensors for extended periods while engaging in daily activities is not practical. As a solution, our previous work proposed a calibration method for accelerometers attached to the chest using a mask sensor [16]. Chest movement was measured with an accelerometer and calibrated to the actual respiration volume recorded by the mask sensor. However, the output of the accelerometer heavily depends on its orientation relative to gravitational acceleration, which limits measurement accuracy.

Recently, wearable devices integrated into textiles have represented a groundbreaking advancement in the field of wearable technology, combining the comfort and familiarity of clothing with sophisticated health monitoring capabilities [21–23]. These smart textiles incorporate flexible sensors and electronic components directly into fabrics, allowing for seamless integration into everyday clothing items such as shirts, socks, and even underwear. By embedding sensors that can monitor various physiological parameters, these textiles transform ordinary garments into powerful health monitoring tools. Taking advantage of such devices, here we propose a calibration of a wearable piezoelectric thread for quantitative monitoring of respiration.

In practical usage, both the wearable piezoelectric thread and the mask sensor are initially worn together on the body and face, respectively, as illustrated in Figure 1. The wearable piezoelectric thread outputs are then quantitatively calibrated using the respiratory frequency and volume measured by the mask sensor. Once this calibration is completed, the mask can be displaced, and the wearable sensor can independently monitor quantitative respiration information during daily activities. The utilization of a piezoelectric mechanism is also crucial to limit energy consumption since piezoelectric sensors can output electrical potential fluctuations without any power supply. This study focuses on the proof-of-concept unraveling the correlation between the physical movement of the body surface and the airflow produced during respiration.
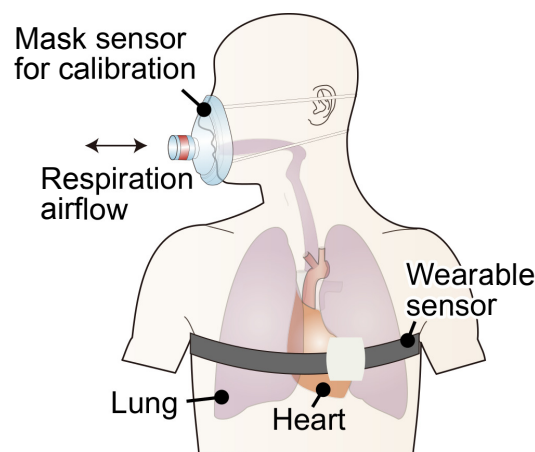

Figure 1. Schematics of the piezoelectric thread sensor utilized in this study.

2. Sensor Preparation

2.1. Piezoelectric Thread Sensor

A commercially available piezoelectric thread sensor (PIEZOLA™, Mitsui Chemicals, Inc., Tokyo, Japan) was utilized in this study. The thread has a diameter of 700 μm as illustrated in Figure 2. Inside the outer polytetrafluoroethylene (PTFE) insulation layer, there is a poly(L-lactic acid) piezoelectric film (μFLEX™, Mitsui Chemicals, Inc.) sandwiched in between Cu foils. The Cu foils work as electrodes while the structure is similar to the typical coaxial cable.
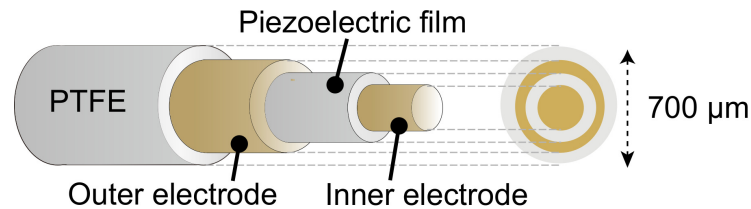

Figure 2. Schematics of the piezoelectric thread sensor utilized in this study.

The sensing mechanism relies on the piezoelectricity of the sandwiched film [21]. Polarization occurs between the surfaces when stress is applied to the film. Such polarization produces a potential difference between the electrodes. According to the datasheet, the film itself is reported to generate 4–5 V in response to 1 N of application force. This mechanism allows voltage generation between the electrodes when the thread is deformed, without requiring any driving voltage input. The piezoelectric thread can endure tensions of up to 13 N, with a linear stress–strain relationship of up to 1% elongation. Under such testing conditions, it exhibits a stable linear output with a sensitivity per unit length of 14 pC N^{-1} mm^{-1}, consistent from room temperature up to 60 °C [21]. The thread was directly connected to a coaxial cable to read the released potential.

2.2. Airflow Sensor

A tube airflow rate sensor as illustrated in Figure 3 was fabricated using a standard lift-off microfabrication process. The detail of the fabrication process was explained in our previous publication [24]. The serpentine sensing structure was fabricated on a polyimide (PI) film. The film sensor was rolled and fixed at the inner wall of a tube package, enabling measurement of the airflow rate passing through the tube. The measurement is based on the resistance–temperature relationship of the metallic serpentine structures.
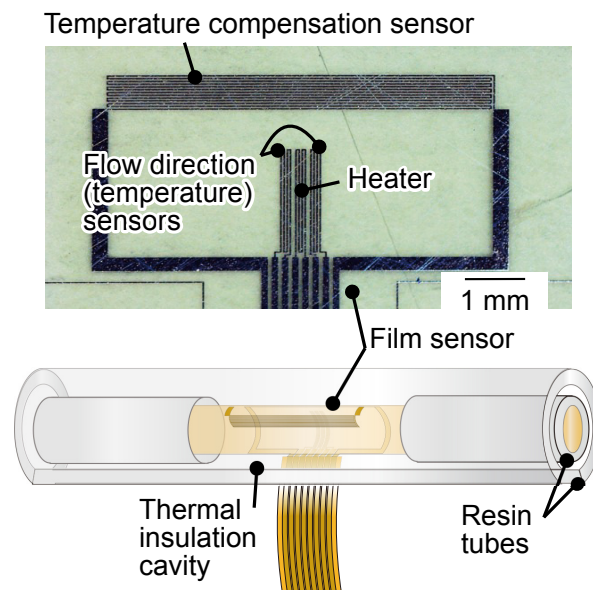

Figure 3. Schematics of the tube airflow rate sensor utilized in this study.

The airflow rate sensor worked based on a hot-wire thermal anemometry with a temperature compensation element. A heater was patterned at the heart of the structure. During measurement, the heater was heated up at a constant temperature using a feedback circuit. In the presence of airflow, the heat dissipated from the heater. This causes the feedback circuit to supply extra current, which maintains the heater temperature at a constant level. Here, the amount of heat dissipated is proportional to the airflow velocity. The airflow velocity can be converted to airflow rate using the defined tube inner diameter.

To measure the airflow direction, a thermal calorimetry mechanism was utilized. A pair of temperature sensors was positioned, one upstream and one downstream relative to the heater. In the absence of airflow, the heat dissipated from the heater was symmetrically distributed between the temperature sensors, resulting in a similar sensor output canceling each other. In the presence of airflow, the heat dissipated downstream, causing an increase in the differential of the temperature sensor readout. The difference was used to determine the airflow direction.

The basic characteristics of the sensor were characterized by supplying airflow with a controlled rate using a commercially available mass flow controller (Model 3200, Kofloc Corp., Kyoto, Japan). The sensing characteristic is shown in Figure 4. The anemometry characteristic of the sensor, shown in Figure 4a, followed the theoretical King's model [25], as expressed in Equations (1) and (2) for the forward and reverse directions, respectively. The equations are indicated as solid lines in the graph.

$$V^2 = 0.4048 + 0.0039u^{0.7} \tag{1}$$

$$V^2 = 0.4052 + 0.0048u^{0.65} \tag{2}$$

Here, u expresses the airflow rate input, where V is the sensor readout. The calorimetry characteristic of the sensor shown in Figure 4b indicates that the sensor can distinguish the airflow direction. The basic characteristic was used to convert the sensor readout to airflow rate output in the following proof-of-concept experiment.
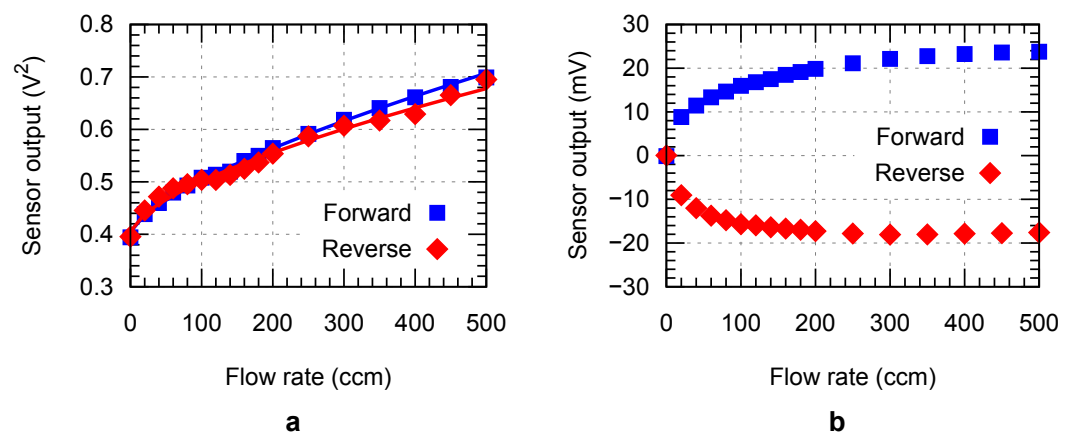

Figure 4. Calibration measurement of the fabricated airflow rate sensor: (**a**) Anemometry response for airflow rate measurement, and (**b**) calorimetry response to distinguish airflow direction.

3. Proof-of-Concept Experiment

The proof-of-concept experiment was performed using an artificial ventilator (Small Animal Ventilator Model 683, Harvard Apparatus, Cambourne, UK), which simulates human respiration activity. The setup is illustrated in Figure 5. The piston movement of the artificial ventilator resembles the human chest motion during respiration, while the airflow produced by the ventilator resembles human respiration airflow. The piezoelectric thread sensor was anchored to a static point on the floor at one end and to the piston at the other end. This condition corresponds to the utilization of the sensor on the human chest. Meanwhile, the airflow sensor tube was fixed on the outlet of the ventilator to measure the output airflow. This corresponds to the measurement of airflow at the mouth. The

piston was operated at different frequencies of 0.5, 1.0, and 2.0 Hz to simulate various respiration conditions.

Measurement results for the 0.5 Hz ventilator operation frequency are indicated in Figure 6a. The corresponding piston movement conditions are illustrated in Figure 6b. Here, each cycle was broken down into four phases in accordance with the relation between the airflow and piston movement. During phase (1), the air was inhaled into the ventilator while the piezoelectric thread was stretched. In phase (2), the piston turned its movement direction, causing the air to be exhaled from the ventilator while the piezoelectric thread was gradually relaxed. During the following phase (3), the piston moved in the same direction, and the air was continuously exhaled from the ventilator while the piezoelectric thread was stretched. In the final phase (4), the piston turned its movement direction causing the air to be inhaled while the piezoelectric thread was gradually relaxed.

The maximum output of the piezoelectric sensor was obtained around the position when the piston translated its movement from pulling to pushing or vice versa. This is due to the sensing mode switching from tension to relaxation following the drastic velocity change indicated by piston movement and flow rate direction reversal. Before the direction switching, the piston velocity decreased as reflected by the airflow rate steep decrease at the end of phase (1). The significant deceleration was measured as the maximum negative output of the piezoelectric sensor, indicating the deceleration of the stretching. During the transition, when the airflow rate was zero, the piezoelectric sensor output also returned to zero, indicating an instantaneous stop of the piston to reverse its direction. Next, the piston started to accelerate significantly in the opposite direction at the beginning of phase (2) as indicated by the steep rise of the airflow rate. This acceleration was measured as the maximum positive output of the piezoelectric sensor at the early phase (2), indicating the acceleration of its relaxation. The same phenomena occurred around the position when the airflow direction changed from positive to negative in phases (3) and (4), resulting in a similar piezoelectric sensor output.

Meanwhile, when the piston passed the equilibrium point—the position where the piezoelectric sensor was least stretched—the sensor experienced a mode switch from relaxation to tension. This mode switching was marked by small spikes in the piezoelectric sensor output, corresponding to the maximum flow rate output. Around this switching point, the airflow rate change, i.e., acceleration or deceleration, was not as significant as in the previously mentioned cases. This was indicated by the gentle inclination angle at the interface between phases (2) and (3). Therefore, piezoelectric sensor peaks were not as large as in the previous cases. In accordance with this behavior, the piezoelectric sensor output was considered equivalent to the measure of flow rate change. Integration of the magnitude yielded a waveform similar to the flow rate waveform; however, it was blind to direction, as shown in Figure 6a.

Measurement results for ventilator operation frequencies of 1.0 Hz and 2.0 Hz are shown in Figures 7a and 7b, respectively. The piezoelectric sensor output demonstrated similar behavior to the flow rate at higher frequencies, indicating a similar operation mode. The absolute magnitude of the piezoelectric sensor output increased with the operation frequency, likely due to the faster piston movement generating a higher flow rate. Integration of the magnitudes also produced a waveform similar to the flow rate waveform but with direction blindness.

Respiration involves bidirectional airflow, which can be measured quantitatively by the airflow sensor. However, the piezoelectric sensor indicated a direction blindness. Considering that inhalation and exhalation occur consecutively, which means that the airflow direction shifts after approaching its zero value, the inhalation and exhalation should be defined by the user before the utilization of this sensor in practical application.

In Figure 8, the piezoelectric sensor output is plotted against the output airflow rate when the artificial ventilator was operated at a 1 Hz frequency. Figures 8a and 8b indicate the correlation at negative and positive airflow rates, respectively. Considering the direction blindness of the piezoelectric sensor output, the absolute flow rate was extracted and plotted against the piezoelectric sensor output as shown in Figure 8c. A linear approximation equation, as summarized in Equation (3), was derived as the correlation between both magnitudes. Here, y_1 represents the integrated magnitude of the piezoelectric sensor output, and u denotes the flow rate.

$$y_1 = 2.88 \times 10^{-3}|u| - 1.105 \tag{3}$$

According to the correlation plot, the presence of hysteresis can be observed. The coefficient of determination R^2 of the linear approximation equation was 0.833. This indicates a linear correlation between both magnitudes, showcasing the potential of the sensor for quantitative respiration measurement.

The measurement obtained from the piezoelectric thread was then utilized to extract the flow rate using Equation (3). The result is indicated in Figure 9. Tidal volume can be calculated by integrating the flow rate with respect to time. The integration of the final positive peak (marked in gray) in Figure 9 resulted in 8.09 cc. Meanwhile, the direct measurement of tidal volume using the airflow sensor shown in Figure 7a was 7.63 cc. The proposed method successfully measured tidal volume with an error of less than 10% error.

Figure 10 shows the correlation between the absolute flow rate measurement with the integration of piezoelectric sensor output under different artificial ventilator operation frequencies. Linear approximations of the correlations at 0.5 Hz and 2 Hz artificial ventilator operation frequencies are presented mathematically in Equations (4) and (5), respectively. The coefficients of determination of the equations were 0.823 and 0.719, indicating adequate accuracy.

$$y_{0.5} = 4.27 \times 10^{-3}|u| - 2.236 \tag{4}$$

$$y_2 = 1.58 \times 10^{-3}|u| - 0.783 \tag{5}$$

The offset difference between each measurement can be attributed to the different initial positions of the piston during the measurement. Meanwhile, the gradient difference indicates the frequency dependence of the correlation between the flow rate and the piezoelectric sensor output. The gradient of the approximation equation decreased with the operation frequency. Therefore, the utilization of each correlation equation can be selected based on the breathing frequency that can be measured simultaneously.
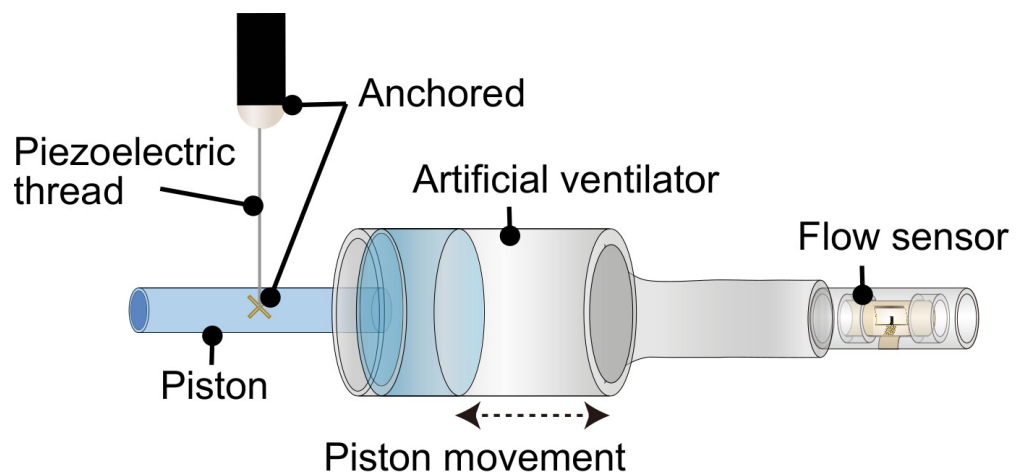

Figure 5. Proof-of-concept experimental setup using an artificial ventilator.
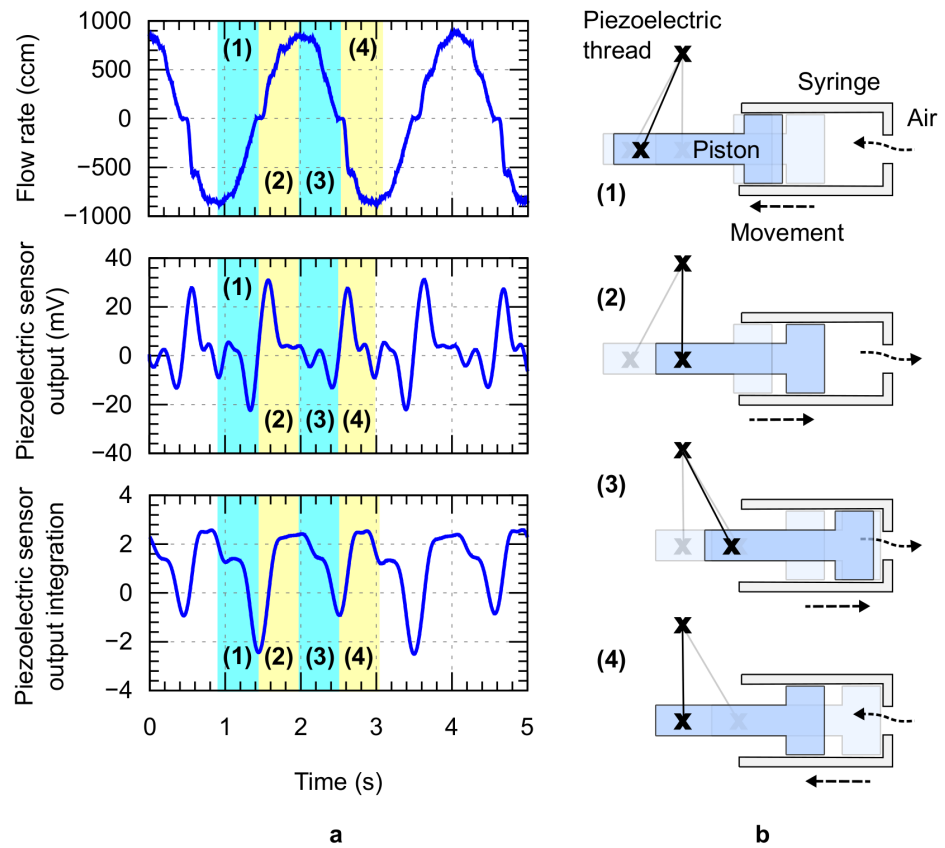
Figure 6. (**a**) Proof-of-concept experimental results under a 0.5 Hz ventilator operation condition: Output airflow rate, piezoelectric thread sensor output, and the integration of the piezoelectric thread output. (**b**) Schematics of ventilator movement conditions during each phase shown in (**a**).
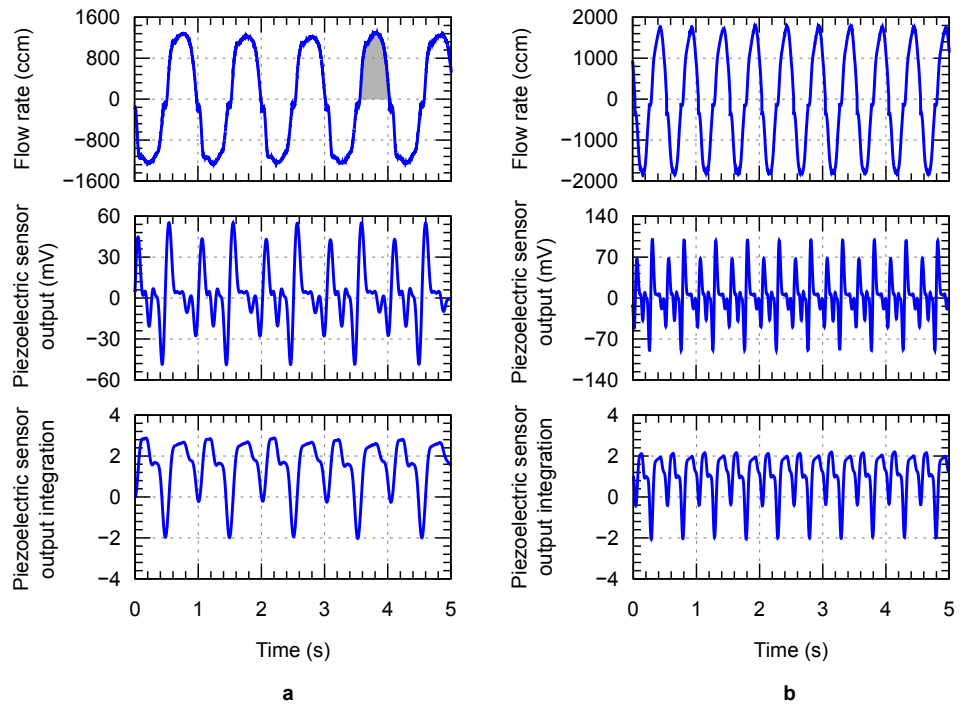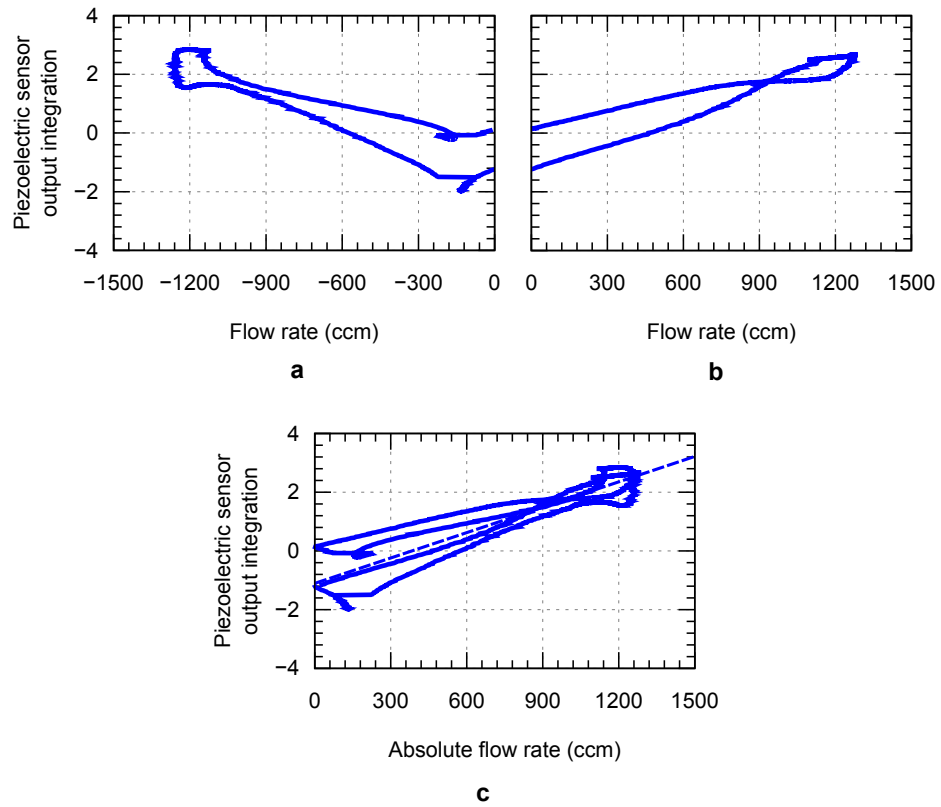

Figure 7. Proof-of-concept experimental results under (**a**) 1.0 and (**b**) 2.0 Hz ventilator operation conditions: Output airflow rate, piezoelectric thread sensor output, and integration of the piezoelectric thread output.

Figure 8. Correlation between output airflow and integration of the piezoelectric sensor under (**a**) negative, (**b**) positive, and (**c**) absolute airflow rates with a 1 Hz artificial ventilator operation frequency. The dashed line indicates the mathematical approximation equation.
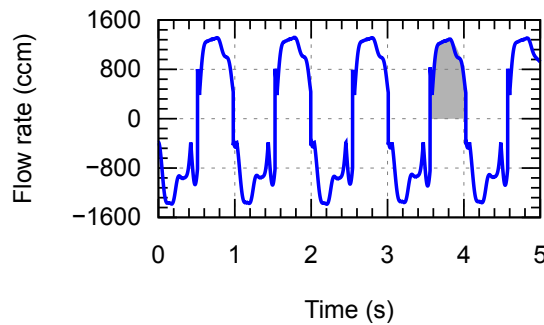
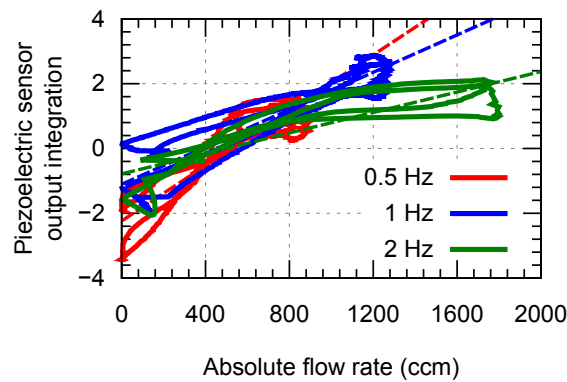**Figure 9.** Airflow rate from the piezoelectric thread sensor measurement.

Figure 10. Correlation between the absolute airflow rate and integration of the piezoelectric sensor under different artificial ventilator operation frequencies. Dashed lines indicate mathematical approximations.

4. Conclusions

To enable quantitative respiration monitoring using textile sensors, we proposed a calibration method for a wearable piezoelectric thread using airflow measured at the mouth. The correlation between the piezoelectric sensor output and airflow was investigated in a proof-of-concept study employing an artificial ventilator. The ventilator's piston movement resembled chest movement, while the output airflow corresponded to respiration activity. The piezoelectric thread was attached to the piston, while a miniaturized tube airflow sensor was embedded in the outlet of the ventilator. We confirmed that the first integration of the piezoelectric output correlated well with the airflow rate. Using the piezoelectric thread, tidal volume measurement with an error of less than 10% was achieved after implementing the proposed calibration method. The correlation revealed in this study enabled quantitative respiration monitoring using the textile sensor. Future studies will include the development of algorithms for hysteresis compensation along with clinical experiments. The robustness of the method, considering slight displacement during attachment, will be evaluated in clinical experiments.

The integration of respiration monitoring into wearable devices not only enhances the ability to detect and manage respiratory diseases but also promotes proactive health management by allowing individuals to monitor their breathing in real-time. This continuous stream of data facilitates early intervention, potentially preventing the escalation of respiratory issues and improving overall health outcomes. The convenience and unobtrusiveness of wearable respiration sensors promote consistent use, offering healthcare providers a comprehensive and accurate view of a patient's respiratory health over time. As technology advances, the role of wearable sensors in respiration monitoring and overall health management is set to become increasingly significant, paving the way for more personalized, efficient, and effective healthcare solutions.

References

1. Lou, Z.; Wang, L.; Jiang, K.; Wei, Z.; Shen, G. Reviews of wearable healthcare systems: Materials, devices and system integration. *Mater. Sci. Eng. R. Rep.* **2020**, *140*, 100523. [CrossRef]
2. Ding, X.; Clifton, D.; Ji, N.; Lovell, N.H.; Bonato, P.; Chen, W.; Yu, X.; Xue, Z.; Xiang, T.; Long, X.; et al. Wearable Sensing and Telehealth Technology with Potential Applications in the Coronavirus Pandemic. *IEEE Rev. Biomed. Eng.* **2021**, *14*, 48–70. [CrossRef]
3. Ates, H.C.; Nguyen, P.Q.; Gonzalez-Macia, L.; Morales-Narváez, E.; Güder, F.; Collins, J.J.; Dincer, C. End-to-end design of wearable sensors. *Nat. Rev. Mater.* **2022**, *7*, 887–907. [CrossRef]
4. Vanegas, E.; Igual, R.; Plaza, I. Sensing Systems for Respiration Monitoring: A Technical Systematic Review. *Sensors* **2020**, *20*, 5446. [CrossRef]
5. Rosso, M.; Nastro, A.; Baù, M.; Ferrari, M.; Ferrari, V.; Corigliano, A.; Ardito, R. Piezoelectric Energy Harvesting from Low-Frequency Vibrations Based on Magnetic Plucking and Indirect Impacts. *Sensors* **2022**, *22*, 5911. [CrossRef]

6. Shikida, M.; Hasegawa, Y.; Al Farisi, M.S.; Matsushima, M.; Kawabe, T. Advancements in MEMS technology for medical applications: Microneedles and miniaturized sensors. *Jpn. J. Appl. Phys.* **2022**, *61*, SA0803. [CrossRef]

7. Al Farisi, M.S.; Wang, Y.; Hasegawa, Y.; Matsushima, M.; Kawabe, T.; Shikida, M. Facile In-Tube-Center Packaging of Flexible Airflow Rate Microsensor for Simultaneous Respiration and Heartbeat Measurement. *IEEE Sensors J.* **2023**, *23*, 12626–12633. [CrossRef]

8. Mannino, D.M.; Buist, A.S. Global burden of COPD: Risk factors, prevalence, and future trends. *Lancet* **2007**, *370*, 765–773. [CrossRef]

9. Heldt, G.P.; Ward, R.J. Evaluation of Ultrasound-Based Sensor to Monitor Respiratory and Nonrespiratory Movement and Timing in Infants. *IEEE Trans. Biomed. Eng.* **2016**, *63*, 619–629. [CrossRef]

10. Dinh, T.; Nguyen, T.; Phan, H.P.; Nguyen, N.T.; Dao, D.V.; Bell, J. Stretchable respiration sensors: Advanced designs and multifunctional platforms for wearable physiological monitoring. *Biosens. Bioelectron.* **2020**, *166*, 112460. [CrossRef]

11. Karlen, W.; Raman, S.; Ansermino, J.M.; Dumont, G.A. Multiparameter respiratory rate estimation from the photoplethysmogram. *IEEE Trans. Biomed. Eng.* **2013**, *60*, 1946–1953. [CrossRef] [PubMed]

12. Wang, X.; Ke, Z.; Liao, G.; Pan, X.; Yang, Y.; Xu, W. A Fast-Response Breathing Monitoring System for Human Respiration Disease Detection. *IEEE Sensors J.* **2022**, *22*, 10411–10419. [CrossRef]

13. Adiono, T.; Ahmadi, N.; Saraswati, C.; Aditya, Y.; Yudhanto, Y.P.; Aziz, A.; Wulandari, L.; Maranatha, D.; Khusnurrokhman, G.; Riadi, A.R.W.; et al. Respinos: A Portable Device for Remote Vital Signs Monitoring of COVID-19 Patients. *IEEE Trans. Biomed. Circuits Syst.* **2022**, *16*, 947–961. [CrossRef] [PubMed]

14. Mahbub, I.; Pullano, S.A.; Wang, H.; Islam, S.K.; Fiorillo, A.S.; To, G.; Mahfouz, M.R. A Low-Power Wireless Piezoelectric Sensor-Based Respiration Monitoring System Realized in CMOS Process. *IEEE Sensors J.* **2017**, *17*, 1858–1864. [CrossRef]

15. Ohkura, N.; Tanaka, R.; Watanabe, S.; Hara, J.; Abo, M.; Nakade, Y.; Horii, J.; Matsuura, Y.; Inoue, D.; Takata, M.; et al. Chest dynamic-ventilatory digital radiography in chronic obstructive or restrictive lung disease. *Int. J. COPD* **2021**, *16*, 1393–1399. [CrossRef] [PubMed]

16. Horie, K.; Al Farisi, M.S.; Hasegawa, Y.; Matsushima, M.; Kawabe, T.; Shikida, M. Investigation of Calibration Methodology Using Mouth Airflow for Wearable Sensor Toward Quantitative Respiration Monitoring. *IEEJ Trans. Electr. Electron. Eng.* **2024**, *19*, 800–806. [CrossRef]

17. Hermawan, A.; Amrillah, T.; Riapanitra, A.; Ong, W.J.; Yin, S. Prospects and Challenges of MXenes as Emerging Sensing Materials for Flexible and Wearable Breath-Based Biomarker Diagnosis. *Adv. Healthc. Mater.* **2021**, *10*, 1–27. [CrossRef]

18. Jiang, T.; Deng, L.; Qiu, W.; Liang, J.; Wu, Y.; Shao, Z.; Wang, D.; Zhang, M.; Qian, X.; Zhong, J.; et al. Wearable breath monitoring via a hot-film/calorimetric airflow sensing system. *Biosens. Bioelectron.* **2020**, *163*, 112288. [CrossRef]

19. Johns, D.P.; Walters, J.A.E.; Haydn Walters, E. Diagnosis and early detection of COPD using spirometry. *J. Thorac. Dis.* **2014**, *6*, 1557–1569. [CrossRef]

20. Zhou, P.; Yang, L.; Huang, Y.X. A smart phone based handheld wireless spirometer with functions and precision comparable to laboratory spirometers. *Sensors* **2019**, *19*, 2487. [CrossRef]

21. Yoshida, M.; Onishi, K.; Tanimoto, K.; Nishikawa, S. Flexible tension sensor based on poly(l-lactic acid) film with coaxial structure. *Jpn. J. Appl. Phys.* **2017**, *56*, 10PG02. [CrossRef]

22. Karita, M.; Kumagai, S.; Sasaki, M. Respiration monitoring during 6 min walk using wearable sensor measuring capacitance built across skin. *Jpn. J. Appl. Phys.* **2022**, *61*, SA1010. [CrossRef]

23. Al Farisi, M.S.; Wang, Y.; Hasegawa, Y.; Shikida, M. Facile Packaging for Fiber-Shaped Flexible MEMS Thermal Accelerometer. *IEEE Sensors Lett.* **2023**, *7*, 2504704. [CrossRef]

24. Hasegawa, Y.; Kawaoka, H.; Mitsunari, Y.; Matsushima, M.; Kawabe, T.; Shikida, M. Catheter type thermal flow sensor with small footprint for measuring breathing function. *Microsyst. Technol.* **2018**, *24*, 3455–3465. [CrossRef]

25. King, L.V. XII—On the convection of heat from small cylinders in a stream of fluid: Determination of the convection constants of small platinum wires with applications to hot-wire anemometry. *Philos. Trans. R. Soc. London. Ser. A Contain. Pap. A Math. Phys. Character* **1914**, *214*, 373–432. [CrossRef]